Hindawi
Advances in Materials Science and Engineering
Volume 2022, Article ID 5685372, 15 pages
https://doi.org/10.1155/2022/5685372

Research Article

Fresh, Mechanical, and Microstructural Properties Investigation on the Combined Effect of Biomedical Waste Incinerator Ash and Bagasse Ash for High-Strength Concrete

Menker Girma [1,2] **and Belachew Asteray** [2]

[1]*Department of Construction Technology and Management, Institute of Technology, Debre Markos University, Debre Markos, Ethiopia*
[2]*Department of Civil Engineering, College of Architecture and Civil Engineering, Construction Quality & Technology Center of Excellence, Addis Ababa Science and Technology University, Addis Ababa, Ethiopia*

Correspondence should be addressed to Menker Girma; menker.girma@aastu.edu.et

Received 16 December 2021; Revised 23 March 2022; Accepted 20 April 2022; Published 31 May 2022

Academic Editor: Teresa M. Piqu

The combination effect of supplementary cementitious materials in the production of high-strength concrete production is an effective way to reduce the amount of cement required while contributing to environmental sustainability and cost. This study aims to assess the microstructural investigation on the combined effect of biomedical waste incinerator ash (BWIA) and bagasse ash (BA) as a partial replacement of cement in high-strength concrete production. The cement was partially replaced with BA (0%, 2.5%, 5%, and 7.5%) and BWIA (0%, 2.5%, 5%, and 7.5%). The mix design was done as per the ACI 211-4R-93 mix design standard. Slump, slump flowability, density, and compaction factor tests were conducted for freshly mixed concrete. Mechanical properties of the hardened concrete from four different mixes were also determined for the 7- and 28-day cured specimens. The microstructural properties of the hardened concrete for all mixes were also investigated using scanning electron microscopy (SEM) and X-ray diffraction (XRD) tests. Based on the experimental results, the compressive strength of high-strength concrete at every 2.5% BA and 2.5% BWIA replacement of cement in the concrete mix at 7 days of curing was slightly decreased, while at 28 days of curing, the compressive strength of the control mix (51.8 MPa) decreased as compared to the mix codes' compressive strength of the BWIA and BA5 and BWIA and BA10 mix codes, at 54.8 MPa and 52.5 MPa, respectively. The SEM micrographs showed that the partial replacement of cement by the BWIA and BA leads to a decrease in the pore proportion in the enlarged interfacial transition zone (ITZ), reduced CH crystals, and a denser C–S–H gel as compared to the control specimen. The XRD pattern showed the existence of portlandite, ettringite, okenite, quartz, and calcite in the cement and aggregate phases. As a result, the usage of BWIA and BA has a significant impact on the properties of high-strength concrete in fresh, hardened, and microstructure high-strength concrete.

1. Introduction

Concrete is the most widely used construction material in the world because it is a multipurpose material that can be used to construct a variety of structures such as buildings, roads, dams, bridges, and so on. It is a composite material composed of Portland cement, coarse aggregate, fine aggregate, water, air, and occasionally used admixture [1, 2]. High-strength concrete is designed to greater compressive strength, flexural strength, and greater splitting strength than normal concrete. To create high-strength concrete that must meet performance criteria standards, superior materials are employed. To produce high-strength concrete, special mixing, placement, and curing methods are required [3]. The assembly of concrete-making ingredients or materials generally requires high cost and high energy and

hence is a source of environmental pollution. Green concrete is distinguished by the use of industrial byproducts, agricultural byproducts, or alternative materials to conserve biodiversity, save money and energy, and reduce environmental effects [4–8].

Cement manufacturing contributes about 5% to 8% of global man-made CO_2 emissions. About half of the emissions are caused by process emissions during the clinker manufacture, 40% by the combustion of fuels to heat the cement kiln, and 10% by power consumption and transportation [3, 6, 9–14] As a result, reducing carbon dioxide (CO_2) emissions from cement production is a critical and urgent task for the cement industry. Energy efficiency through modern dry-process technology, the use of other fuels to replace coal and pet coke within the cement kiln heating process, the substitution of clinker with other mineral components in cement, and determining other cement replacing potential materials are the four main handles for CO_2 reduction. The partial substitution of cement mix ratio is often done by biomedical waste incinerator ash and bagasse ash in concrete production to stop hazardous effects on the environment [14–16]. Biomedical waste generation has risen significantly over the past decades, with an annual increase of 8%. Incineration has increased in importance as an alternative method of reducing the dimensions of biomedical waste, resulting in the production of ash as a reduced volume of waste. It has been utilized as a partial replacement for cement in concrete production and as a road subgrade material in various countries. Effective use of biomedical waste ash would not only reduce the cost of construction but also contribute significantly to the reduction of environmental risks [15, 17–23]. When used as a supplementary cementitious material in a cement mix, biomedical waste ash also acts as a pozzolanic material because it contains a high percentage of calcium oxide, CaO, SiO_2, and Al_2O_3, 40.21%, 20.1%, and 11.13% of the main component of medical waste ash, respectively [22].

Ethiopia was constructing the eight primary medical waste incinerator centers as well as pharmaceutical and clinical waste disposal facilities, and the machines were installed in Adama, Mekele, Bahir Dar, Dessie, Jimma, Neqemte, Hawassa, and Dire Dawa. Waste is thermally decomposed in several chambers of the incinerator machine using an oxygen-deficient medium-temperature combustion process in an 800–900°C chamber. Incinerators in the postcombustion chamber use air heated to 900–1200°C to reduce smoke and odor. The incineration center, which was installed in Adama, has a capacity to burn one thousand kilograms of medical waste per hour, while the remainder burns five hundred kilograms of waste per hour. The machines have a working time of 20 hours [24]. According to the Ethiopian public health institution 2018 annual report, annual medical waste in Ethiopia is above 93,000 tons. Nowadays, it is obvious that the number of healthcare facilities, governmental and nongovernmental hospitals, health centers, and health stations in Ethiopia is growing, implying that the amount of healthcare pharmaceutical wastes generated by these institutions would eventually increase.

When used as a supplementary cementitious material to the cement mix, bagasse ash also acts as a pozzolanic material property because it has a high percentage of silica (SiO_2), which reacts with the cement mix to form calcium silicate-hydrate gel during the hydration process. This extra C–S–H improves the mechanical strength of cement mortar and concrete, as well as the bonding between cement paste and aggregates, or the microstructure of concrete [14, 25–27]. Annual sugarcane production in Ethiopia is approximately 350,000 tons, so the potential for sugarcane bagasse ash is approximately 84,000 tons. According to Ethiopia's growth transformation plan, 4.6 million tons of sugar would be produced annually, resulting from the assembly of more than 1.1 million tons of sugar cane bagasse ash as waste. This amount of waste is often beneficial when utilized for a variety of productive purposes. It is used as a supplementary cementitious material in the production of concrete [28]. Based on their results, those hard waste materials partially replaced with cement significantly improved the engineering and performance properties of concrete. In addition to these waste materials, there are also abundantly available solid waste materials generated by the sugarcane manufacturing industry and medical waste incineration centers that harm human beings and the environment as well; this is termed sugarcane bagasse ash and biomedical waste incineration ash.

The experimental results on the rheological and mechanical strength characteristics of concrete recommend that up to 15% bagasse waste ash and 10% biomedical waste ash be used as a partial replacement for the weight of Portland cement in the mix to produce high-quality concrete. According to their findings, the hard waste components that were partially replaced with cement enhanced the technical and performance qualities of concrete significantly. In addition to these waste materials, there are abundantly available solid waste materials generated by the sugarcane manufacturing industry and medical waste incineration centers that have an adverse influence on humans and the environment; these are known as sugarcane bagasse ash and biomedical waste ash waste. Therefore, the objective of this study is to conduct a microstructural investigation on the combined effect of biomedical waste incinerator ash and bagasse ash for high-strength concrete.

2. Material and Methods

2.1. Materials. The materials used in the present study are cement, water, fine and coarse aggregate, bagasse ash (BA), biomedical waste incinerator ash (BWIA), and high range water reducer (HRWR) admixture.

2.1.1. Cement. Locally produced Dangote OPC 42.5 R cement was used and its quality was tested as per the ASTM C150/C150 M standard specification [29].

2.1.2. Fine Aggregate. River sand was used as a fine aggregate purchased from a locally available market. It was carefully washed with water to remove the silt and debris in it.

Physical laboratory tests were conducted according to the ASTM standard specification. The term fine aggregate is used for particles smaller than 4.75 mm sieve size [30]. The percentage of passing was found between the lower and upper limits of the ASTM C 33–08 standard specification. The particle size distribution of the fine aggregate is shown in Figure 1(b). The physical properties of the fine aggregate material used in the present study are summarized in Table 1.

2.1.3. Coarse Aggregate. It was purchased from the YEN-COMADE Construction PLC crusher plant found in Goro, Addis Ababa, Ethiopia. The shape, size, and quality of coarse aggregate are important factors in the production of high-strength concrete. The material's physical properties were tested according to the ASTM standard specification. According to [30], the term coarse aggregate is used to describe particles larger than the 4.75 mm sieve size. The coarse aggregate particle size distribution of coarse aggregate is shown in Figure 1(a) and the percentages of passing were found between the lower and upper limit of the ASTM C 33–08 standard specification. The physical properties of the coarse aggregate material used in the present study are summarized in Table 2.

2.1.4. Biomedical Waste Incinerator Ash (BWIA). It was obtained from Adama Medical Waste Incineration Center, Adama, Ethiopia. The BWIA was obtained from the burning of biomedical waste from various medical institutes such as hospital health centers, health stations, and pharmaceuticals waste, which is burnt in incineration center by using high temperature of 800–1200°C. The physical properties of the BWIA material used in the present study are summarized in Table 3. A sample finer than 150 μm sieve was used and its chemical compositions were determined in the Ethiopian geological survey complete silicate laboratory. The results are summarized in Table 3. The total sum of $(SiO_2 + Al_2O_3 + Fe_2O_3)$ is equal to 52.08%. The calcium oxide, CaO, is 29.86%, and the iron oxide Fe_2O_3 content is 1.08%. As a result, according to ASTM C 618–08a, this ash is classified as a class C pozzolan. Figure 2 illustrates the Adama Medical Waste Incineration Center and BWIA samples finer than 150 μm.

2.1.5. Bagasse Ash (BA). The bagasse ash used in the study was obtained from the Wonji Sugar Factory, Wonji, Oromia Regional State, Ethiopia. The BA was obtained after the removal of sugar juice from sugar cane bagasse and then transferred to a certain chamber to be burnt by a very high temperature of 600–900 C; thus the ash is produced. The physical properties of the BA material used in the present study are summarized in Table 3. Its chemical compositions were determined in the Ethiopian geological survey complete silicate laboratory, and the results are summarized in Table 4. The total quantity of $(SiO_2 + Al_2O_3 + Fe_2O_3)$ is 82.28%, which is more than the minimum ASTM C 618–08a standard for class F, which is 70%. Calcium oxide, CaO, has a value of 1.44%, and iron oxide, Fe_2O_3, has a value of 4.32%. As a result, this ash is categorized as a class F pozzolan by ASTM C 618–08a. Figure 3 illustrates the open storage of bagasse ash at the Wonji Sugarcane Factory and BA samples finer than 150 μm.

2.1.6. Water. Potable water from the laboratory, free from organic substances, was used for mixing and curing prepared samples.

2.1.7. Water-Reducing Admixtures. Water-reducing admixtures are important to reduce the quantity of mixing water to produce high-strength concrete with a definite slump, decrease water to cement ratio, and reduce the amount of cement. Typical water reducers condense the water content by almost 5% to 15%. Locally produced water-reducing admixtures were used for this present study.

2.2. Sampling. Sampling is that a comparatively small number of units if selected in a manner that sincerely represents the study sample, can provide with a sufficiently high degree of probability a fairly true reflection of the sampling population that is being studied [31, 32]. Purposive sampling, which is a random sample method, was used in this study. In this study, BA, BWIA, and other ingredients samples are sampled based on purpose-sampling techniques.

2.3. Mix Design. In the present study, the C-50 grade of concrete was designed according to ACI 211-4R-93. Four mixtures of concrete mixes were prepared with a water-cement ratio of 0.34. With cement, the mix ration was partially replaced with bagasse ash (0%, 2.5%, 5%, and 7.5%) and biomedical waste incinerator ash (0%, 2.5%, 5%, and 7.5%). The mix proportion designed for high-strength concrete mix is shown in Table 5.

2.4. Test Methods

2.4.1. Fresh and Hardened Concrete Tests. The properties of both fresh and hardened concrete are determined as per the ASTM standard specifications. The study was carried out in the construction materials laboratory of Addis Ababa Science and Technology University, Addis Ababa, Ethiopia. The workability of fresh concrete is examined through a slump, slump flowability, compaction factor, and the density of fresh concrete. The details of fresh concrete tests are shown below (Figure 4 and 5).

(1) Slump test is the most common test for determining the consistency of freshly mixed concrete. The fresh concrete mix slump test process, apparatus, and detailed measured values were determined by ASTM C-143 standard procedures [33]. Figure 4(a) showed the slump test.

(2) The flowability test of freshly mixed concrete was performed in accordance with ASTM C-1611 requirements, but without using a J-Ring [34]. The

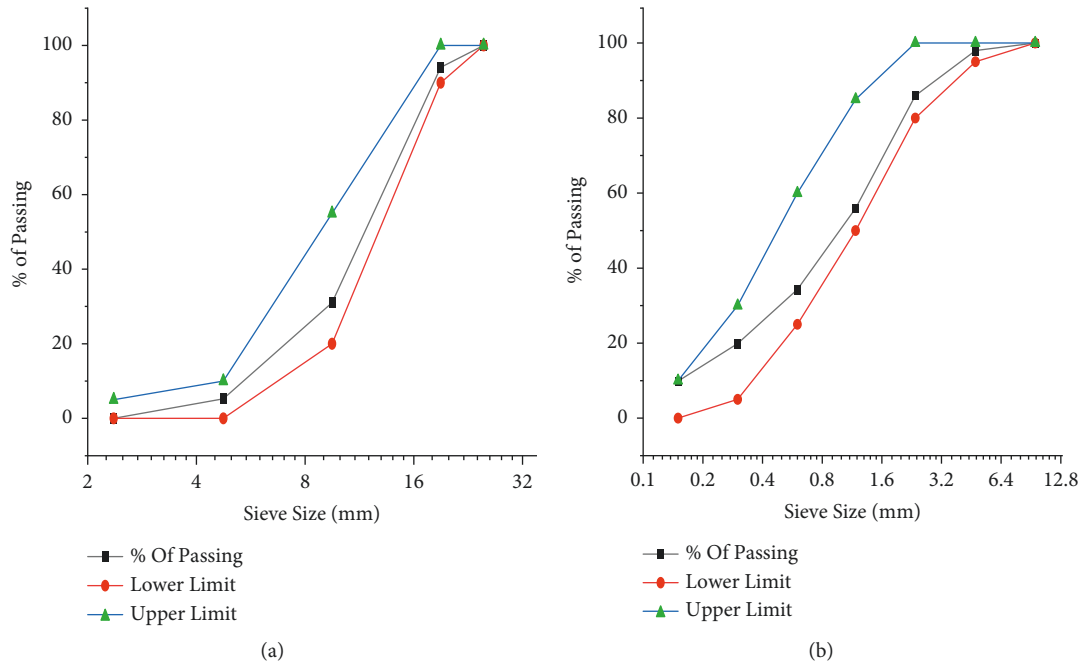

Figure 1: (a) Gradation of coarse aggregate, (b) gradation of fine aggregate.

Table 1: Physical properties of fine aggregate.

Properties	Test result	Standards	ASTM requirement	Remark
Fineness modulus	2.96	ASTM-C136	2.5 to 3.0	Ok
Bulk unit weight	1,634 kg/m^3	ASTM-C29	1200–1750 kg/m3	Ok
Specific gravity	2.75	ASTM-C128	2.4 to 2.9	Ok
Absorption capacity	2.03%	ASTM-C128	<4%	Ok
Moisture content	4.17%	ASTM-C566	3–8%	Ok
Silt content	3.46%	ASTM-C40	>3%	—

Table 2: Physical properties of coarse aggregate.

Physical properties	Test result	Standards	ASTM requirement	Remark
Bulk unit weight	1660 kg/m^3	ASTM-C29	1200 to 1750 kg/m^3	Ok
Specific gravity	2.88	ASTM-C127	2.30 to 2.90	Ok
Absorption capacity	1%	ASTM-C127	0.5 to 4%	Ok
Moisture content	0.83%	ASTM-C566	1–6%	Ok

Table 3: Physical properties of OPC (42.2 grade), BA, and BWIA.

Properties	OPC	BA	BWIA	Standards
Finesses	94.03%	92.94%	90.57%	ASTM C -184
Specific gravity	3.20	2.18	2.54	ASTM C -188

following equation has been used to calculate slump flow (flowability): Figure 4(b) displayed the flowability test of freshly mixed concrete.

$$\text{Slump Flow}\,(cm) = \frac{(d1 + d2)}{2}, \quad (1)$$

where $d1$ is the largest diameter of the resulting circular flow of concrete (cm); $d2$ is a second diameter of the circular flow approximately perpendicular to the first measured diameter ($d1$) (cm).

(3) The compaction factor test more accurately measures the workability of concrete. It provides the techniques for determining the compaction factor of concrete with and without cement replacement by BA and BWIA. It was performed as per ACI 211-3–75 standard specifications. The following equation

(a) (b)

Figure 2: (a) BWIA Incineration Center, (b) BWIA sample finer than 150 μm.

Table 4: Chemical properties of OPC (42.2 grade), BA, and BWIA.

Materials	SiO_2	Al_2O_3	Fe_2O_3	CaO	MgO	Na_2O	K_2O	MnO	P_2O_5	TiO_2	H_2O	Loi
OPC	20.84	4.72	3.35	65.88	2.08	0.26	0.61	—	—	—	—	0.87
BA	68.54	9.42	4.32	1.44	0.92	1.56	7.84	0.16	0.76	0.14	0.80	3.70
BWIA	34.34	16.66	1.08	29.86	3.76	1.80	0.76	0.04	0.72	0.49	2.39	7.70

(a) (b)

Figure 3: (a) Dumping of BA in the open environment, (b) BA sample finer than 150 μm.

Table 5: Mix design proportion per kg/m3 with cement replacement material.

Mix code	Cement (Kg)	BA		BWIA		CA (kg)	FA (kg)	Water with (HRWR, 3OZ) (kg)
		%	Kg	%	Kg			
BWIA&BA 0	529	—	—	—	—	1,188.5	584.81	182.40
BWIA&BA 5	502.6	2.5	13.2	2.5	13.2	1,188.5	584.81	182.40
BWIA&BA 10	476.1	5	26.45	5	26.45	1,188.5	584.81	182.40
BWIA&BA 15	449.7	7.5	39.68	7.5	39.68	1,188.5	584.81	182.40

was used to calculate the compaction factor: Figure 4(c) showed the compaction factor test of freshly mixed concrete.

$$\text{The Compaction Factor}\,(C.F) = \frac{W2 - W1}{W3 - W1}, \quad (2)$$

where $W1$ is the weight of unfilled cylinder (Kg), $W2$ is the weight of partially compacted concrete (Kg), and $W3$ is the weight of completely compacted concrete (Kg).

(4) The density of fresh concrete was determined as per the ASTM C-1688 standard specification [35]. The

(a) (b) (c)

Figure 4: (a) Slump test, (b) flowability test, (c) compaction factor test.

(a) (b) (c)

Figure 5: (a) Compressive strength test, (b) split tensile strength test, and (c) flexural strength test.

density of freshly mixed concrete with and without cement replacement by BA and BWIA was calculated using the following equation:

$$\text{The density of fresh concrete}\left(\frac{Kg}{m3}\right) = \frac{W2 - W1}{\text{volume of cylinder}}, \tag{3}$$

where $W1$ is the weight of unfilled cylinder (Kg) and $W2$ is the weight of completely compacted concrete (Kg).

(5) Three basic tests were conducted for hardened high-strength properties. The details of each test are explained as follows.

(6) The compressive strength was tested on concrete size cubes of 15*15*15 cm after 7 and 28 days of curing; it was performed according to [36] standard. Figure 5(a) showed the compressive strength test. The compressive strength test result was calculated using the following equation:

$$CS = \frac{F}{A}, \tag{4}$$

where CS is compressive strength (N/mm^2), F is failure load (KN), and A is cross-sectional area (mm^2).

(7) The split tensile strength was tested in cylindrical samples with dimensions ∅ 15*30 cm after curing a total of 7 and 28 days. Figure 5(b) shows split tensile strength test. This test procedure, apparatus, and detailed calculated values were determined according to ASTM C-496 standard methods [37]. The split tensile strength test result was calculated by the following equation:

(a) (b)

Figure 6: (a) JCM-6000 Plus Bench Top SEM JEOL machine. (b) Model XRD-7000 XRD machine.

$$T = \frac{2P}{\pi LD}, \quad (5)$$

where T is splitting tensile strength (MPa), P is maximum applied load (KN), L is length (mm), and D is diameter (mm).

(8) The flexural strength was tested with the size 10*10*50 cm after 28 days of curing. The flexural strength test specimens were prepared and cured according to the ASTM C-78 standard [38]. The result of the flexural strength test was calculated by the following equation. Figure 5(c) showed the flexural strength test.

$$R = \frac{PL}{b\ d^*d}, \quad (6)$$

where R is modulus of rupture (MPa), P is maximum applied load (KN), L is span length, mm, b is average width of a specimen (mm), and d is average depth of specimen (mm).

2.4.2. Microstructure Test. Microstructure examinations of the high-strength concrete were performed on the 28-day cured failed compressive strength specimens for the control (without BA and BWIA), BA and BWIA 5%, BA and BWIA 10%, and BA and BWIA 15% mix code. The cube samples are crushed and the hardened cement paste is collected from the innermost core of the concrete cube samples. The collected samples were then sieved through a 150 μm sieve size. After the preparation of the samples, the test was conducted for scanning electron microscopy (SEM) and X-ray diffraction (XRD) analysis. The study was carried out in the microbiology and material engineering laboratories of Adama Science and Technology University, Adama, Ethiopia. The range of scale utilized in SEM analysis was 20 μm with a resolution of x 1000 and 500 μm with an x 500 magnification rate. The microstructural analysis of four cement paste powder samples is pictured by the JCM-6000 Plus Bench Top SEM JEOL machine, the machine shown below in Figure 6(a).

The mineralogical composition of hydrate concrete powder was investigated by X-ray diffraction (XRD) using a machine produced by Shimadzu Corporation (Japan), model XRD-7000, as shown in Figure 6(b). They have an X-ray tube target fitted with a Cu terminal. The samples were scanned for operating voltages of 40.0 (kV) and current of 30.0 (mA), a divergence of 1.000 (deg), and a receiving slit of 0.3000 (mm), respectively. The measurement conditions were the scanning mode drive axis Theta-2Theta, scan range degree of 10–60 (deg) continuous, speed of 3.0000 (deg/min), sampling pitch of 0.0200 (deg), and a preset time of 0.40 (sec). The phase identification was determined using Match software (Match! Copyright 2003–2021 Bonn, Germany) (Crystal Impact) [36, 37].

3. Result and Discussions

3.1. Effect of BA and BWIA on Fresh Concrete Properties. The qualities of fresh concrete are important. Consistency and workability of fresh concrete are significant requirements for the proportion of concrete mixes as well as important features that impact the placing of fresh concrete on-site and the subsequent performance of hardened concrete [39]. Various tests are conducted to analyze the properties of freshly mixed concrete, such as the slump test, slump flowability, compaction factor, and density of freshly mixed concrete. The results of each test are presented and discussed below.

A slump test method was used to determine the workability of freshly mixed high-strength concrete. This concrete mixture should be workable. It should be simple to place, compact, and complete. As shown in Figure 7(a), the slump of freshly mixed high-strength concrete with and without replacement of the cement mix ratio by bagasse ash and biomedical waste incinerator ash results in varying slumps of 120 to 97 mm. Values of 120–97 mm are considered high slumps. According to Harsimranpreet Kaur et al. [23], increasing the replacement amount of biomedical waste incinerator ash in the cement mix ratio decreases the slump of freshly mixed concrete. Similarly, in the present study, the replacement percentage of bagasse ash and

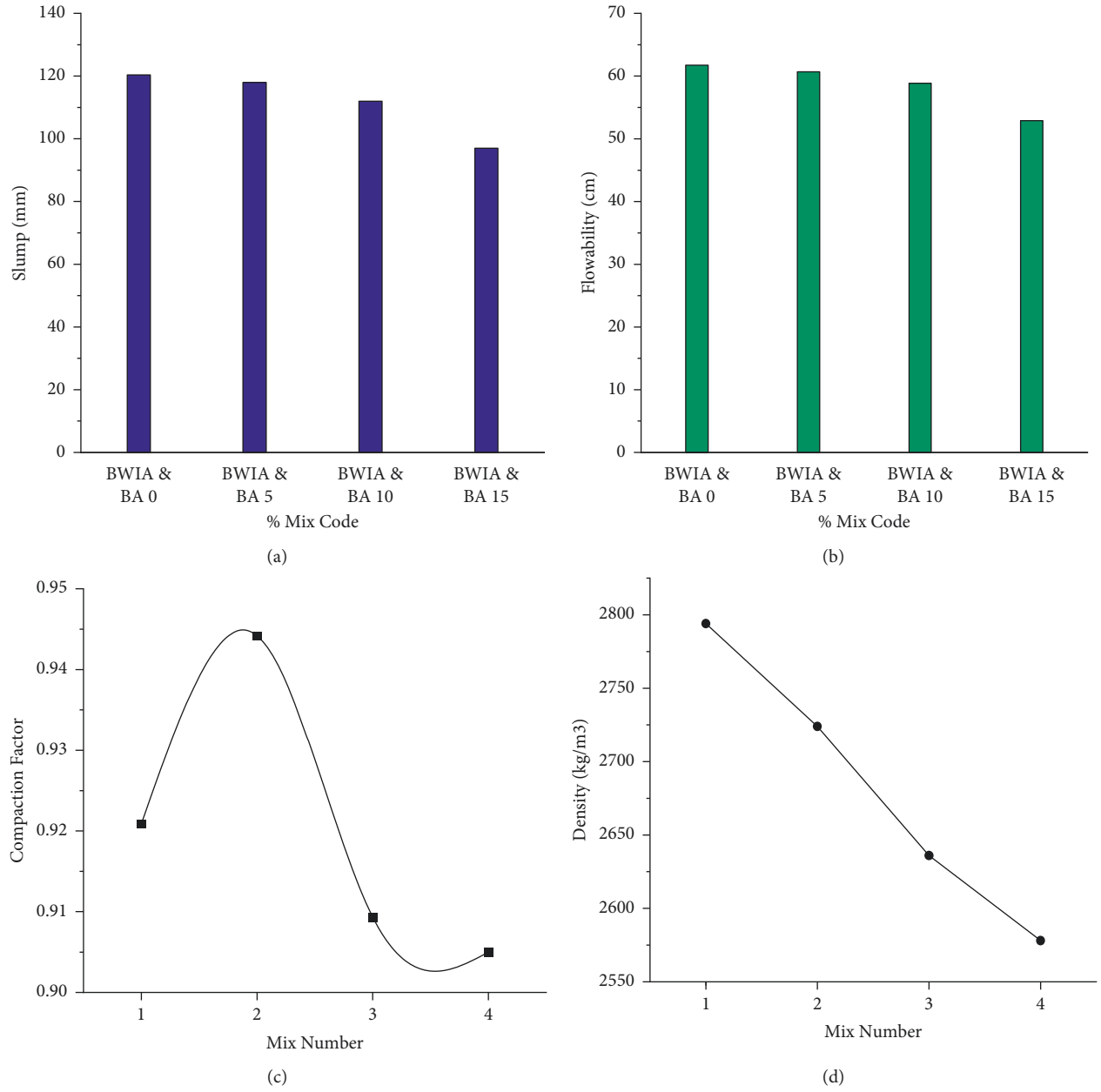

Figure 7: Fresh concrete properties tests: (a) slump teste result; (b) slump flowability test result; (c) compaction factor test result; (d) density test result.

biomedical waste incinerator ash increased as the slump declined. This was accomplished due to the holey nature and uneven shape of BWIA and BA particles.

The slump test was not appropriate for the analysis of the fluidity of the high-strength concrete. The slump flowability test is also an actual indicator of extreme bleeding and segregation of concrete mix. As can be inferred from Figure 7(b), the flowability test result of freshly mixed concrete is shown. All four mixes were satisfied with the high-strength concrete flowability range between 50 cm and 65 cm [40]. The last mix flowability is 52.9 cm, thus satisfying the range of flowability of high-strength concrete, but compared to the control mix, it is 8.9 cm less because the percentage of replacement is 7.5% BA and 7.5% BWIA, which is higher than the first two mixes. The percentage of replacement of bagasse ash and biomedical waste incinerator ash increases the flowability of concrete decrease.

Figure 7(c) shows the compaction factor test result of freshly mixed concrete. This is the most appropriate test for concrete that has a low water-cement ratio (high-strength concrete). The concrete compaction factor ranges between 0.78 and 0.95, where the test results vary between 0.90 and 0.94. Mix numbers 1, 3, and 4 are medium workability, and mix number 2's compaction factor is 0.94. The compaction factor of the control mix is lower than that of the mix in which the ordinary portland cement partially replaced with

2.5% BA and 2.5% BWIA. The value indicates that the workability is higher compared to the control mix, increasing the quantity of cement and reducing the percentage of replacement of bagasse ash and biomedical waste incinerator ash to increase the compacting factor value.

The combined effect of bagasse ash and biomedical waste incinerator ash replacement on freshly mixed concrete density is shown in Figure 7(d). At every percentage replacement of cement with bagasse ash and biomedical waste incinerator ash mix, density is decreased as compared to the control mix density because the specific gravity of cement (3.20) is higher than the specific gravity of BA and BWIA (2.18 and 2.54, respectively) as shown in Table 3. Similarly, according to Jugal V. Tailor et al. [15], there is an increase in the replacement quantity of biomedical waste ash in the cement mix ratio while the density of concrete decreases.

3.2. Effect of BA and BWIA on Hardened Concrete Properties. The effect of a partial replacement bagasse ash and biomedical waste incinerator ash to cement mix ratio on hardened concrete properties is investigated and shown in Figure 8(a)–8(c). Hardened concrete properties are determined in terms of compressive strength, split tensile strength, and flexural strength.

The compressive strength tests were performed at 7 and 28 days of curing for the control mix and each percentage of replacement mix. High-strength concrete compressive strength without and with replacement of cement by bagasse ash and biomedical waste incinerator ash is shown in Figure 8(a). At 7 days of curing, the compressive strength of the control mix was higher than the mix with the replacement of BA and BWIA for all percentages. Without the replacement of cement by BA and BWIA there is a better early compressive strength due to the high fineness of cement and the fact that pozzolanic materials hydrate slowly. At 28 days of curing, the compressive strength of the control mix decreases compared to the BWIA and BA5 and BWIA and BA10 mix code compressive strength, which have been observed to be 55 MPa and 53 MPa; because of the fineness and chemical composition of ordinary Portland cement, the hydration processes are faster at an early age. After 7 days, the hydration processes become much slower, and the hydration processes of bagasse ash and biomedical waste incinerator ash increase. According to Pritish Gupta Quedou et al. [14, 18, 39, 41] the compressive strength increases with curing time but decreases as the proportion of pozzolanic materials replacement increases. Therefore, the compressive strength of the study decreases as the replacement of BA and BWIA increases.

The split tensile strength test after 7 and 28 days of curing is shown in Figure 8(b). At 7 days of cured split tensile strength, the result varies from 2.15 MPa to 3.73 MPa and after 28 days of curing, the variation is between 3.08 MPa and 4.49 MPa. The split tensile strength decreases in the early days of curing with BA and BWIA. This was attributed to the high porosity and lower finesses of BA and BWIA. At 28 days of cure age, the replacement of cement with 2.5% BA and 2.5% of BWIA showed the highest split tensile strength compared to the control mix. According to ACI Committee 363R-10, the splitting tensile strength is almost 5% to 10% of the compressive strength of concrete and 70% of the flexural tensile strength after 28 days of curing [42]. The split tensile results of all concrete mixes at 7 days and 28 days of curing were compatible with 5% to 10% of the compressive strength of concrete and 70% of the flexural tensile strength at 28 days of curing. According to Bashir Ahmed Memon et al. [16, 17], increasing the replacement quantity of biomedical waste ash in the cement mix ratio decreases the split tensile strength. Similarly, in this study, 10% and 15% of replacement of BA and BWIA are directly proportional to decreased splitting tensile strength.

Figure 8(c) shows the flexural strength test results of the high-strength concrete on 28 days of cured specimens. The results show that all high-strength concrete mixes recorded high flexural strength. The flexural strength of the concrete decreased as the amount of BA and BWIA was increased. Replacement of OPC with 2.5% BA and 2.5% BWIA showed the highest flexural strength compared to the control mix. Higher flexural strengths are a function of higher compressive strengths. When the proportion of replacement of pozzolanic material replacement increases, the flexural strength decreases [14, 16].

3.3. XRD Analysis. X-ray diffractometer (XRD) is a nondestructive test method for the identification of materials' crystalline phase characterization and mineralogical composition [42–44]. The XRD diffraction patterns of four hydrated concrete powder samples are shown in Figure 9(a)–9(d). X-ray diffraction patterns are formed by a goniometer which is rotated through 10 to 60 degrees of 2theta angles on the samples, with part of the XRD diffraction pattern of hydrated concrete samples. The letter symbols on the figures represent the names of minerals and peak intensities of concrete powder diffraction. The *Y*-axis represented X-ray intensity; the *X*-axis diffraction angle was 2theta degrees. The reference database used in this study was COD-Inorg 2021.06.14. The following X-ray diffraction pattern crystalline phases are covered in this study as portlandite ($Ca(OH)_2$), ettringite (A_{l2} Ca_6 H_{64} O_{50} S_3), calcite ($CaCO_3$), quartz (SiO_2), and okenite (Ca_5 H_{23} O_{32} Si_9), which is similar to the family of C–S–H commonly found in the hardened concrete paste. In all samples, a small amount of calcite is found.

Portlandite is the mineral name for calcium hydroxide [45]. The amount of calcium hydroxide is present in the control mix and blended cement mix with BA (0%, 2.5%, 5%, and 7.5%) and BWIA (0%, 2.5%, 5%, and 7.5%) specimens, which represent an indication of the degree of hydration. The mineral name for this calcium sulfoaluminate is ettringite, which is often found in Portland cement concrete. Supplementary cementitious materials and admixtures also contain sulfate and aluminate. Within the first few hours after mixing with water, gypsum and other sulfate compounds in the cement react with calcium aluminate to create ettringite. The mechanism that controls stiffening is the development of ettringite in fresh concrete, which increases

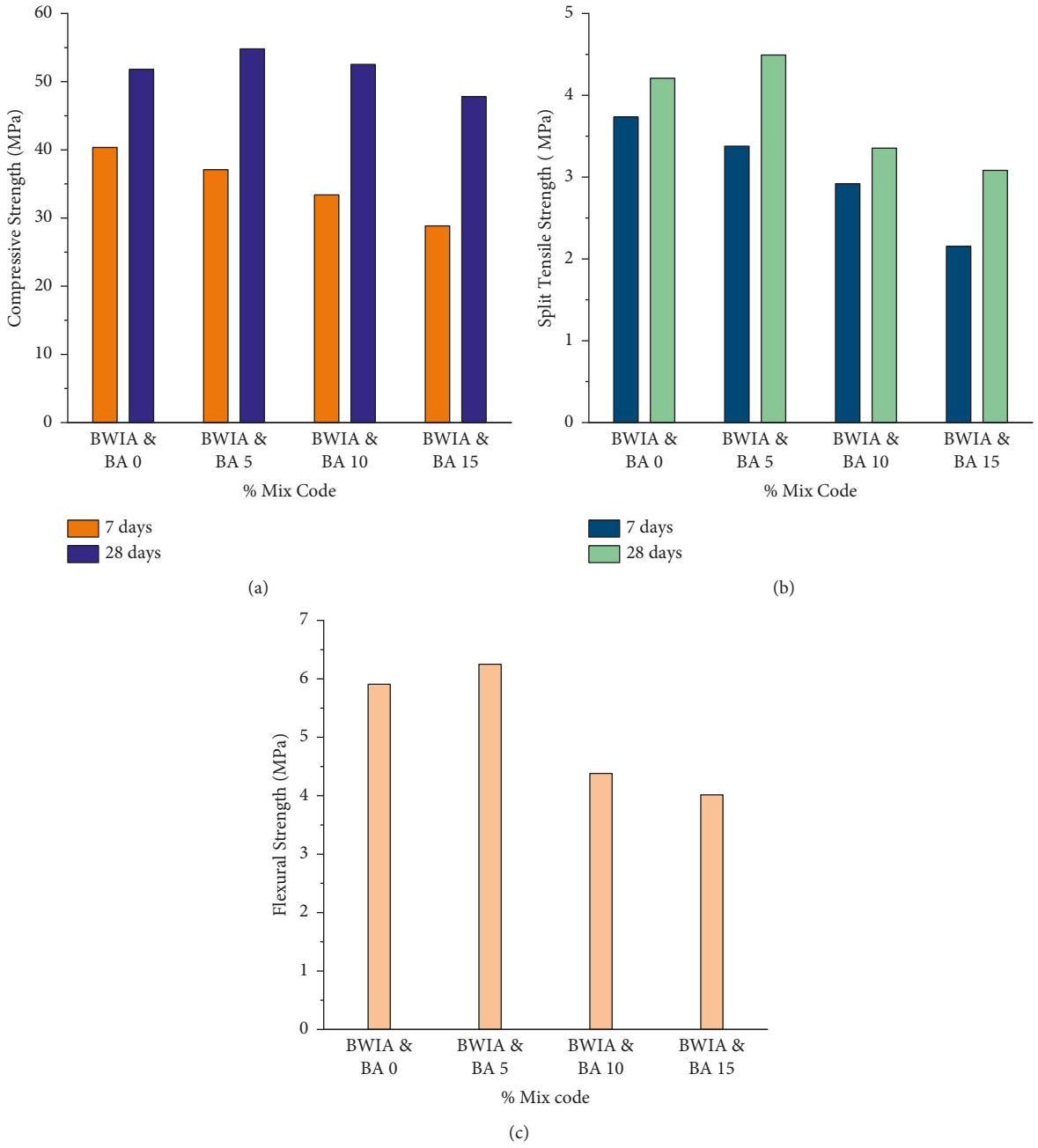

Figure 8: Hardened concrete properties tests: (a) compressive strength test result; (b) split tensile strength test result; (c) flexural strength test result.

strength development, increases durability with filled holes or cracks, and limits drying shrinkage [46]. Silicon oxide is known as quartz (SiO_2). It is the most important part of the sand. It is responsible for the creation of calcium silicates such as dicalcium silicate (C_2S) and tricalcium silicate (C_3S), which are the building blocks of concrete strength. Because of the higher hydration rate, the control mix contains more calcite ($CaCO_3$), has better workability, and has higher compressive strength at an earlier stage of curing than the blended cement mix. However, at 28 days of curing, the compression strength of the control mix decreases due to the higher amount of calcite ($CaCO_3$) and the decreased rate of hydration after 7 days of curing. Similarly, according to Maisarah Ali et al. [47], the present percentage of calcite ($CaCO_3$) increases the workability and early age compressive strength, but increasing the curing age of the concrete decreases compressive strength. Okenite is a hydrated calcium silicate hydroxide. It is an unusual mineral [48]. It frequently forms "cotton ball" collections, where the crystals are so thin that they look like tiny fibers. The collections are composed of straight, radiating, thread-thin crystals. These clusters can make for very attractive specimens and often accompany

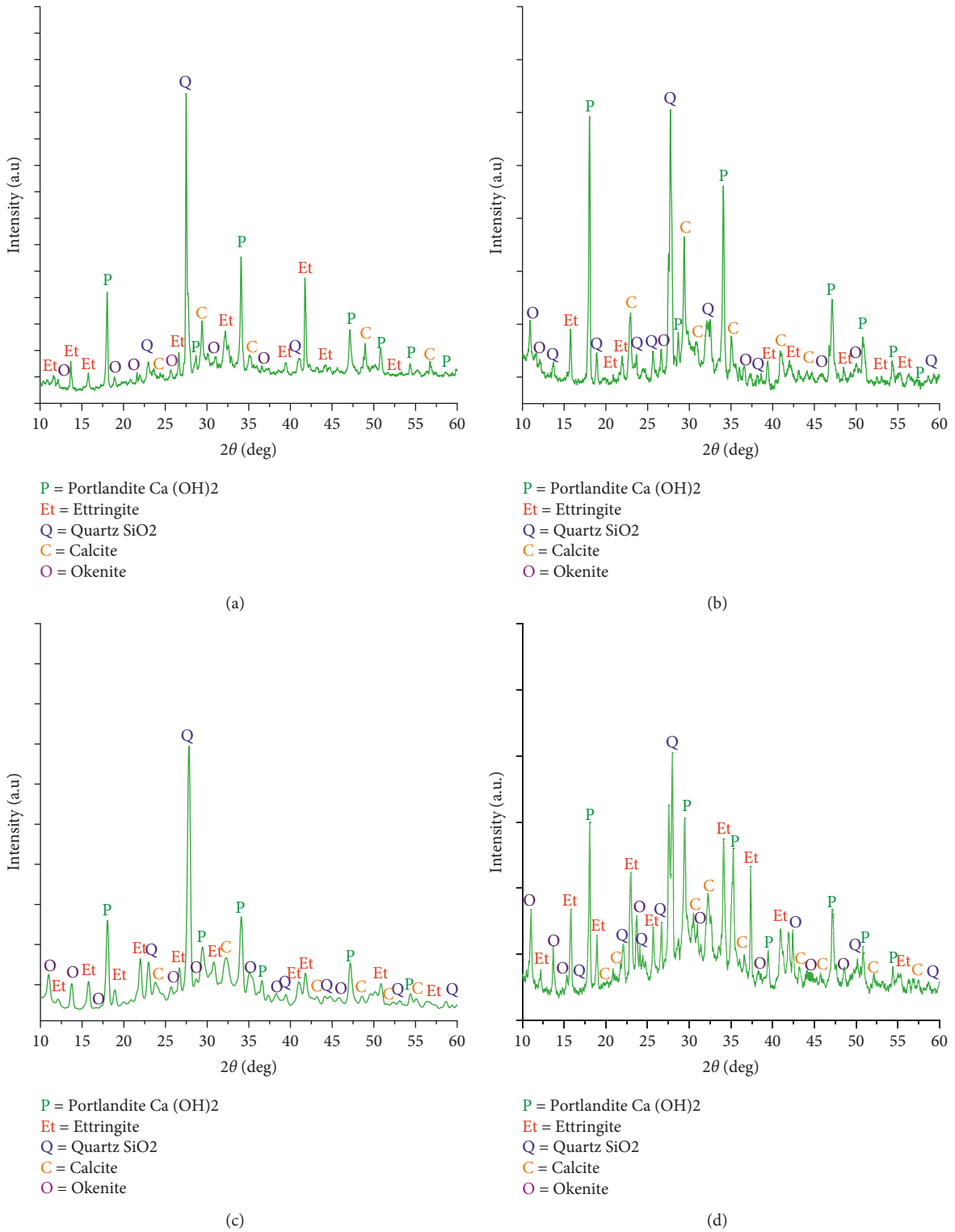

Figure 9: XRD pattern of (a) control mix, (b) 2.5% BA and 2.5% of BWIA mix (BA&BWIA 5), (c) 5% BA and 5% of BWIA mix (BA&BWIA 10), (d) 7.5% BA and 7.5% of BWIA mix (BA&BWIA 15).

many fine and rare minerals such as apophyllite, gyro lite, and many of the zeolites.

The mineralogical composition of the XRD diffraction analysis diffraction pattern graphics of the control mix (BA and BWIA 0) is shown in Figure 9(a). Predominance peaks of quartz ($2\theta = 27.5^{\circ}$), portlandite ($2\theta = 17.9^{\circ}$, 33.7°), and ettringite ($2\theta = 42^{\circ}$) have been observed using XRD analysis. Calcium carbonate (calcite) is present in the mixture as a result of carbon dioxide combined with calcium hydroxides during the mixing and curing processes. All minerals have trigonal (hexagonal) crystal systems in their crystal systems. The XRD diffractometer examination of the diffraction

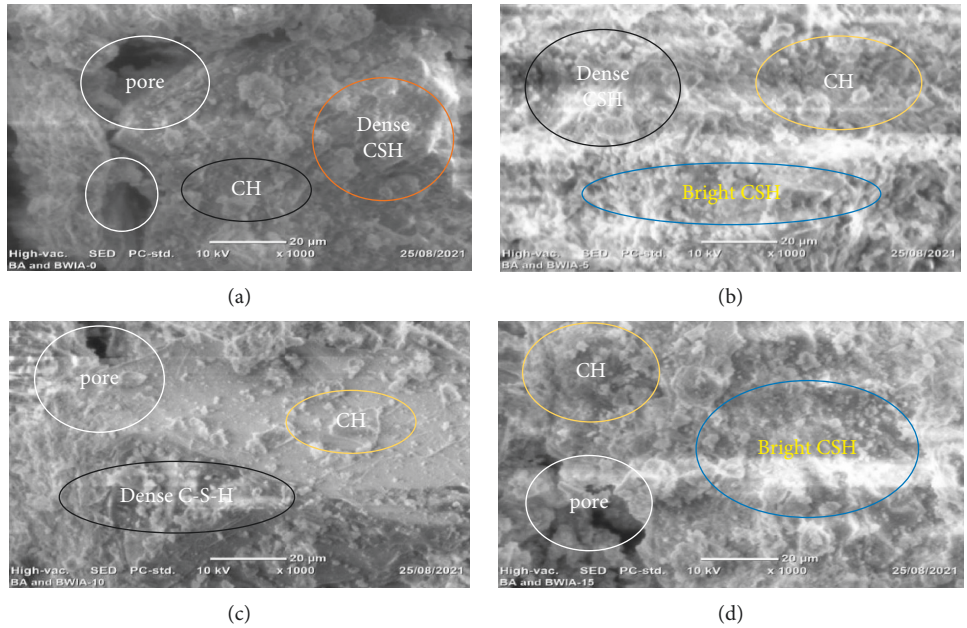

Figure 10: SEM images x1000 magnification rates of (a) control mix, (b) 2.5% of BA and 2.5% of BWIA mix (BA&BWIA 5), (c) 5% of BA and 5% of BWIA mix (BA&BWIA 10), and (d) 7.5% of BA and 7.5% of BWIA mix (BA&BWIA 15).

pattern graphics of the 2.5% BA and 2.5% BWIA mix shows the mineralogical composition of the diffraction pattern graphics in Figure 9(b). The highest peak values of quartz at ($2\theta = 27.5^{\circ}$), portlandite ($2\theta = 17.8^{\circ}$ and 34.4°), and calcite at ($2\theta = 29.7^{\circ}$) have majority peaks, which is formed quickly due to the reaction of calcium hydroxide with the surrounding air carbon dioxide ($Ca(OH)_2 + CO_2 \leftrightarrow CaCO_3 + H_2O$).

Figure 9(c) shows the XRD diffraction pattern graphics for a sample containing a 5% BA and 5% BWIA mix (BA and BWIA 10). The predominance of quartz peak values has been observed around 2theta degrees of 27.5°, while portlandite peak values have been observed around 2theta degrees of 18°. The XRD diffraction pattern graphics of the 7.5% BA and 7.5% BWIA mixes with partial replacement of the cement mix ratio samples are shown in Figure 9(d). The dominant peaks of quartz are 2theta degrees of 27.5°, portlandite is 18° and 30°, and ettringite is 26° and 34.7°.

3.4. SEM Analysis. Concrete has a highly complex and heterogeneous microstructure, which consists of three components such as cement paste, the interfacial transition zone between the cement pastes and aggregates, and the pore's structure. To develop these three components to improve the mechanical strength and durability of high-strength concrete [49], SEM images illustrate the microstructure and surface morphology of C–S–H gel, calcium hydroxide (CH), pores, and ettringite in concrete. The effect of BWIA and BA on the workability, mechanical, and durability properties of concrete can be described by microstructure. When BWIA and BA were partially replaced to cement mix ratio to concrete the size of crystal and pores is smaller, and the bonding between the crystals becomes tighter, which makes the microstructure denser. Figures 10 and 11 show SEM images of the control mix (BA and BWIA 0), 2.5% BA and 2.5% BWIA mix (BA and BWIA 5), 5% BA and 5% BWIA mix (BA and BWIA 10), and 7.5% BA and 7.5% BWIA mix (BA and BWIA 15) cured for 28 days at 20 µm with a resolution of x1000 magnification rate and 50 µm with an x500 magnification rate.

Figures 10(a) and 11(a) show SEM images of the control mix microstructure without partial replacement of BA and BWIA. After 28 days of curing, it is shown that several outstanding blacks are pore structures that are distributed within the control mix samples. It is more permeable when compared to BA and BWIA5, BA and BWIA10, and BA and BWIA15 mix code SEM images. The porosity of concrete has a significant impact on its strength. The pore structure and the structure's limited durability have both contributed to increased permeability.

The micromorphology of the SEM images was presented in Figures 10(b) and 11(b), using a 2.5% BA and 2.5% of BWIA (BA and BWIA 5) combined effect. SEM pictures of this mix do not show visible pores, indicating a denser microstructure than SEM images of the control mix. It indicates that the influence of the pozzolanic reaction changes the pore structure with the decrease in the grain size. The replacement of cement with up to 2.5% of BA and 2.5% of BWIA increases the strength and durability and decreases the permeability of concrete. The bright particles indicate a nonhydrated cement or whiter C–S–H gels around the aggregates. The BA and BWIA in the mix remain unreacted due to the lack of hydration of grain particles in the mix at the age of 28 days, which also needs more curing time to complete the hydration process.

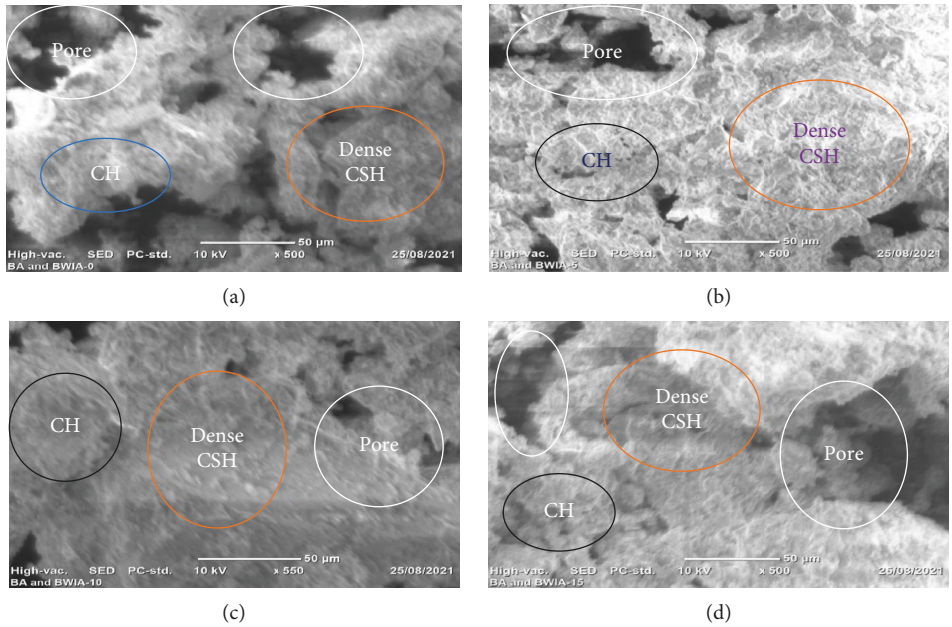

Figure 11: SEM images x500 magnification rates of (a) control mix, (b) 2.5% BA and 2.5% of the BWIA mix (BA&BWIA 5), (c) 5% BA and 5% of the BWIA mix (BA&BWIA 10), and (d) 7.5% BA and 7.5% of the BWIA mix (BA&BWIA 15).

Figures 10(c) and 11(c) show the micromorphology of SEM images with a 5% BA and 5% BWIA mix code (BA and BWIA 10). There is less pore structure compared to the control mix SEM images and the BA and BWIA 15 mix SEM images; therefore, better compressive strength is achieved compared to the control mix compressive strength. The main phases in the microstructure of the hydrated cement mix paste can be seen as hexagonal and cube calcium hydroxide (CH) structures. According to Paul E. Stutzman et al. [50], SEM images show the hexagonal shapes of calcium hydroxide, needle-like is ettringite, and sheet-like is calcium silicate-hydrate. From the SEM image, the microstructure of high-strength concrete is more homogeneous than that of the SEM image of the control mix due to the chemical and physical contributions of BA and BWIA.

In Figures 10(d) and 11(d) shown, the micromorphology of the SEM images was presented with 7.5% BA and 7.5% of BWIA mix (BA and BWIA 15). The darker areas represent pores. Compared to control mix micromorphology, BA and BWIA 15 SEM images have fewer pores. The bright particles indicate that the aggregates are surrounded by a non-hydrated cement or a whiter C–S–H gel. When increasing the partial replacement of cement by BA and BWIA mix curing periods to 28 days, the hydration of cement is not completed. The increased curing periods of 28 days to 56 days and 90 days increase the hydration rate, leading to better mechanical properties for high-strength concrete and the microstructure.

4. Conclusion

The following conclusions were drawn from the experimental results of biomedical waste incinerator ash and bagasse ash properties, effects on fresh and hardened high-strength concrete properties, and microstructure of concrete.

(1) The replacement percentage of BWIA and BA increases the slump, flowability, and compaction factor, and density of fresh concrete decreases.

(2) At an early age of curing, the replacement percentage of BWIA and BA increases compressive strength, and split tensile strength decreases. At 28 days of curing, up to 10% replacement of the BA and BWIA can improve the mechanical properties of high-strength concrete.

(3) According to SEM images, a partial replacement of the cement mix ratio by bagasse ash and biomedical waste incinerator ash results in a denser C–S–H gel with fewer pores than the control mix. Furthermore, improved interlocking between aggregate and cement paste leads to improved mechanical properties in high-strength concrete. Partial replacement of the cement mix ratio by BA and BWIA results in a decrease in the pore proportion in the enlarged ITZ, reduced CH crystals, and a denser C–S–H gel when compared to control mix concrete. XRD could be used to identify the mineralogical components of the hydrated cement paste powder. The XRD data revealed the presence of hydration products like portlandite, ettringite, quartz, calcite, and okenite (hydrated C–S–H), as well as other mineral compounds that would hydrate over time.

Lastly, biomedical waste incinerator ash and bagasse ash are waste products materials from medical waste incinerator centers and the sugarcane industry. Their use as a partial replacement for cement reduces the levels of CO_2 emissions by the cement production process, and their use resolves the disposal problems associated with them in medical waste incinerator centers and sugarcane factories [51–54].

Data Availability

Any data used to support the findings of this study are available from the corresponding author upon request.

Conflicts of Interest

The authors declare that there are no conflicts of interest regarding the report in this paper.

Acknowledgments

The authors express their gratitude to the Adama Science and Technology University microbiology and material engineering laboratory staff for their cooperation with the scanning electron microscopy (SEM) and X-ray diffractometer (XRD) testing.

Supplementary Materials

Figure 1: diffraction pattern graphics of control mix (BA and BWIA 0). Figure 2: diffraction pattern graphics of 2.5& BA and 2.5% of BWIA mix (BA&BWIA 5). Figure 3: diffraction pattern graphics of 5% BA and 5% of BWIA mix (BA&BWIA 10). Figure 4: diffraction pattern graphics of 7.5% BA and 7.5% of BWIA mix (BA&BWIA 15). (*Supplementary Materials*)

References

[1] J. J. B. A. M. Neville, *Concrete Technology*, Vol. 13, UK, Pearson, London, UK, 2 edition, 2010.

[2] P. K. Mehta and P. J. M. Monteiro, *Concrete Microstructure, Properties and Materials*, pp. 1–239, First Edit, Academia Publishing, San Francisco, CA, USA, 2001.

[3] MillionYehualashet, *Experimental Investigation on Mechanical Properties of High-Performance concrete with Partial Replacement of Cement by Fly Ash*, Addis Ababa Science and Technology University, Addis Ababa, Ethiopia, 2019.

[4] G. K. Warati, M. M. Darwish, F. F. Feyessa, and T. Ghebrab, "Suitability of scoria as fine aggregate and its effect on the properties of concrete," *Sustainability*, vol. 11, no. 17, pp. 1–15, 2019.

[5] M. S. Hameed and A. S. S. Sekar, "Properties of green concrete containing quarry rock dust and marble sludge powder as fine aggregate," *ARPN Journal of Engineering and Applied Sciences*, vol. 4, pp. 83–89, 2009, http://www.arpnjournals.com.

[6] M. Syarif, M. S. Kırgız, A. G. D. S. Galdino et al., "Development and assessment of cement and concrete made of the burning of quinary by-product," *Journal of Materials Research and Technology*, vol. 15, pp. 3708–3721, 2021.

[7] N. Bheel, M. O. A. Ali, M. S. Kirgiz, A. G. De Sousa Galdino, and A. Kumar, "Fresh and mechanical properties of concrete made of binary substitution of millet husk ash and wheat straw ash for cement and fine aggregate," *Journal of Materials Research and Technology*, vol. 13, pp. 872–893, 2021.

[8] M. S. Kırgız, "Green cement composite concept reinforced by graphite nano-engineered particle suspension for infrastructure renewal material," *Composites Part B: Engineering*, vol. 154, pp. 423–429, 2018.

[9] FDRE Ministry of Industry, *Ethiopian Cement Industry Development Strategy 2015-2025*, Adiss Ababa, Ethiopia, 2015.

[10] A. Demissew, F. Fufa, and S. Assefa, "Partial replacement of cement by coffee husk ash for c-25 concrete production," *Journal of Civil Engineering, Science and Technology*, vol. 10, no. 1, pp. 12–21, 2019.

[11] Abebe Demissew Gashahun, "Assessment on Cement Production Practice and Potential Cement Replacing Materials in Ethiopia," *Civil and Environmental Research*, vol. 12, pp. 22–28, 2020.

[12] J. Zhang, Y. Zhao, and H. Li, "Experimental investigation and prediction of compressive strength of ultra-high performance concrete containing supplementary cementitious materials," *Advances in Materials Science and Engineering*, vol. 2017, pp. 1–8, 2017.

[13] L. M. Shuhua, J. Wei, Z. Gao, W. Zhou, and Q. Li, "Study on strength and microstructure of cement-based materials containing combination mineral admixtures," *Advances in Materials Science and Engineering*, vol. 2016, p. 10, Article ID 7243670, 2016.

[14] P. G. Quedou, E. Wirquin, and C. Bokhoree, "Sustainable concrete: potency of sugarcane Bagasse ash as a cementitious material in the construction industry," *Case Studies in Construction Materials*, vol. 14, Article ID e00545, 2021.

[15] I. J. V. Tailor and M. Parth, "Department of Civil Engineering, ITM, Universe, Vadodara, "Review on concrete from biomedical waste," *International Journal of Advance Engineering and Research Development*, pp. 36–40, 2017.

[16] S. Praveenkumar and G. Sankarasubramanian, "Mechanical and durability properties of bagasse ash-blended high-performance concrete," *SN Applied Sciences*, vol. 1, no. 12, pp. 1–7, 2019.

[17] O. Mahboob, A. H. B. Bashir Ahmed Memon, and G. Mustafa Khanzada, "Tensile strength of concrete with biomedical waste ash," *World Journal of Engineering Research and Technology WJERT*, vol. 6, no. 5, pp. 81–90, 2020.

[18] S. Sathvik, S. Suchith, A. Edwin, M. Jemimahcarmicheal, and V. Sheela, "Partial replacement of biomedical waste ash in concrete," *International Journal of Innovative Technology and Exploring Engineering*, vol. 8, no. 6S4, pp. 854–857, 2019.

[19] H. Kaur, R. Siddique, and A. Rajor, "Influence of incinerated biomedical waste ash on the properties of concrete," *Construction and Building Materials*, vol. 226, pp. 428–441, 2019.

[20] U. K. Amit Kumar Singh and V. Srivastav, "Biomedical waste ash in concrete : an experimental investigation," *International Journal of Innovative Research in Science, Engineering and Technology*, vol. 5, no. 6, Article ID 11547, 2016.

[21] A. K. S. Udit Kumar and V. Srivastava, "Suitability of biomedical waste ash in concrete," *International Journal of Engineering and Technical Research (IJETR)*, vol. 5, no. 2, pp. 5–8, 2016.

[22] B. Prasanth and V. R. Rao, "Flexural strength and durability of concrete by partial replacement of OPC with biomedical waste ash and metakaolin," *International Journal of Recent Technology and Engineering*, vol. 7, no. 6, pp. 352–358, 2019.

[23] H. Kaur and R. Siddique, "Mechanical and Durability Properties of Concrete Containing Incinerated Biomedical Ash," in *Proceedings of the 10 th International Concrete Congress*, pp. 122–130, Czech Republic, Prague, Sepetember 2019.

[24] B. Ayele, "New medical waste incineration centers come to Ethiopia," vol. 19, 2018, https://Addisfortune.net.

[25] O. Olumide Olu, N. Aminu, and L. Nazif Sabo, "The effect of sugarcane bagasse ash on the properties of Portland limestone cement," *American Journal of Construction and Building Materials*, vol. 4, no. 2, pp. 77–87, 2020.

[26] Q. Xu, T. Ji, S. J. Gao, Z. Yang, and N. Wu, "Characteristics and applications of sugar cane bagasse ash waste in cementitious materials," *Materials*, vol. 12, no. 1, pp. 39–19, 2018.
[27] A. Bazairwe and S. Ainomugisha, "Utilization of sugarcane bagasse ash from power Co-generation boilers as a supplementary cementitious," *Materials*, vol. 2, pp. 1–14, 2021.
[28] T. F. Goshu, *Optimization of Bagasse Ash to Cement Mix Proportion for M30 Grade Concrete*, Addis Ababa Science and Technology University, Addis Ababa, Ethiopia, 2019.
[29] ASTM, *ASTMC150 - 07 and Standard*, ASTM, West Conshohocken, PA, USA, 2009.
[30] ASTM C33-08, "Standard Specification for Concrete Aggregates," ASTM, West Conshohocken, PA, USA, ASTM, West Conshohocken, PA, USA, 2009.
[31] H. J. Seltman, *Experimental Design and Analysis*, 2018.
[32] R. Kumar, *Research Methodology a step-by-step guide for beginners*, SAGE Publications Asia-Pacific Pte Ltd, Singapore, Article ID 048763, 2011.
[33] Astmc143-08, *Standard Test Method for Slump of Hydraulic-Cement Concrete*, http://www.astm.org, 2021.
[34] ASTM C 1611/C 1611M – 05 and Standard, *ASTM C1611-09 Standard Test Method for Slump Flow of Self-Consolidating Concrete*, ASTM, West Conshohocken, PA, USA, 2009, http://www.astm.orgASTM, West Conshohocken, PA, USA.
[35] ASTM C1688/C1688M-08, *Standard test method for density and void content of freshly mixed pervious concrete*, , ASTM, West Conshohocken, PA, USA, 2009, http://www.astm.orgASTM, West Conshohocken, PA, USA.
[36] ASTMC192-07, *Standard Practice for Making and Curing Concrete Test Specimens in the Laboratory*, 2009.
[37] ASTM C496-04, *Standard Test Method for Splitting Tensile Strength of Cylindrical Concrete Specimens1*, ASTM, West Conshohocken, PA, USA, 2008, http://www.astm.orgASTM, West Conshohocken, PA, USA.
[38] ASTM C 78 -08, *Standard Test Method for Flexural Strength of Concrete (Using Simple Beam with Third-Point Loading)*, ASTM, West Conshohocken, PA, USA, 2009, http://www.astm.orgASTM, West Conshohocken, PA, USA.
[39] K. Marar and Ö. Eren, "Effect of cement content and water/cement ratio on fresh concrete properties without admixtures," *International Journal of the Physical Sciences*, vol. 6, no. 24, pp. 5752–5765, 2011.
[40] Japan Society of Civil Engineers, *Standard Specifications for Concrete Structures 'Materials and Construction*Toyoaki MIYAGAWA, 2010, http://www.jsce.or.jp/committee/concrete/e/index.html.
[41] A. S. A. Saran and T. Harish, "Strength and microstructure of sustainable high performance concrete," *International Journal of Recent Technology and Engineering*, vol. 8, no. 4, pp. 4694–4700, 2019.
[42] ACI CommitteeACI 363R-10, *Report on High-Strength Concrete*, http://www.concrete.org, 2015.
[43] P. E. Stutzman, J. W. Bullard, and P. Feng, "Phase Analysis of Portland cement by combined quantitative X-ray powder diffraction and scanning electron microscopy," *Journal of Research of the National Institute of Standards and Technology*, vol. 121, pp. 47–107, 2016.
[44] P. Barnes, *Structure and Performance of Cement*, Taylor & Francis e-Library, New York, NY, USA, 2008.
[45] Z. K. G. International, *Supernatant Nano Graphite Solution for advance Treatment of C Class Fly Ash Cement Systems – Part 2*, 2015.
[46] P. Cement Association, *Ettringite Formation and the Performance of Concrete*, pp. 1–16, 2001.
[47] M. Ali, M. S. Abdullah, and S. A. Saad, "Effect of calcium carbonate replacement on workability and mechanical strength of Portland cement concrete," *Advanced Materials Research*, vol. 1115, pp. 137–141, 2015.
[48] V. S. Marta, "Okenite, CaroSirsO46 ' 18H2O: the first example of a chain and sheet silicate," *American Mineralogist*, vol. 68, no. 4, pp. 614–622, 1983.
[49] A. A. Hilal, "Microstructure of concrete," *High Performance Concrete Technology and Applications*, pp. 3–24, 2016.
[50] P. E. Stutzman, *Scanning Electron Microscopy in Concrete Petrography*, pp. 59–72, National Institute of Standards and Technology, Maryland, MD, USA, 2001.
[51] M. Hafez, M. Kassab, and S. Taha, "Calcination process and kinetic carbonation effect on the hydrated and anhydrate phases of the OPC matrix at early age of hydration," *HBRC Journal*, vol. 17, no. 1, pp. 389–406, 2021.
[52] T. D. Garrett, H. E. Cardenas, and J. G. Lynam, "Sugarcane Bagasse and Rice Husk ash pozzolans: cement strength and corrosion Effects when using saltwater," *Current Research in Green and Sustainable Chemistry*, vol. 1-2, pp. 7–13, 2020.
[53] R. Seyoum, "Investigation on control burned of Bagasse ash on the properties of Bagasse ash-blended mortars," *Materials (Basel)*, vol. 14, no. 17, 2021.
[54] M. E. D. Opper, *X-ray Powder Diffraction XRD for the Analyst*, PANalytical B.V, Netherlands, 2013.